Biophysical Journal Volume 67 October 1994 1370–1386

A Molecular Dynamics Study of Gating in Dioxolane-Linked Gramicidin A Channels

Serge Crouzy,* Thomas B. Woolf,‡ and Benoît Roux‡
*CENG, CEA, Grenoble, France, and ‡Chemistry Department, Université de Montréal, Montréal H3C 3J7 Canada

ABSTRACT The gating transition of the RR and SS dioxolane ring-linked gramicidin A channels were studied with molecular dynamics simulations using a detailed atomic model. It was found that the probable reaction path, describing the transition of the ring from the exterior to the interior of the channel where it blocked the permeation pathway, involved several steps including the isomerization of the transpeptide plane dihedral angle of Val[1]. Reaction coordinates along this pathway were defined, and the transition rates between the stable conformers were calculated. It was found, in good accord with experimental observations, that the calculated blocking rate for the RR-linked channel was 280/s with a mean blocking time of 0.04 ms, whereas such blocking did not occur in the case of the SS-linked channel. An important observation is that the resulting lifetime for the blocked state of the RR-linked channel was in good accord with the experimental observations only when the calculations were performed in the presence of a potassium ion inside the channel.

INTRODUCTION

Controlling the flow of ionic currents is central to the functional role of channel proteins in regulating the movements of charged anions or cations across the cell membrane (Hille, 1984). Direct observation of the electric current flow through individual ion channels with the patch-clamp method has revealed characteristic abrupt transitions between discrete unitary conductance levels (Neher and Sackmann, 1976). These transitions correspond to the "opening" and "closing" of single ion channel macromolecules (Hille, 1984). In the open state, an electrical current can be detected because an energetically favorable pathway is available facilitating the rapid passage of ions through the cell membrane, whereas no current can be detected in the closed state because the permeation pathway is no longer available. Thus, the ion flux through biological ion channels is modulated through the average duration of the open and closed states rather than by an alteration of the magnitude of the maximum transport rate itself (Andersen and Koeppe, 1992; Hille, 1984). An understanding of the microscopic factors involved in the opening and closing of biological channels is therefore of fundamental importance in physiology.

The underlying molecular mechanisms responsible for the opening and closing of macromolecular pores has been the object of much speculation. It is believed that the open and closed states may correspond to different allosteric conformations of the structure forming the pore (Armstrong, 1992; Sigworth, 1994). In the simplest hypothesis, the displacement of a group of atoms, a molecular "gate", is imagined to be effectively responsible for the blocking of the permeation pathway. Some proposed models suggest significant conformational changes of the macromolecular structure, e.g., the "ball and chain model" for the sodium channel (Armstrong, 1981), or the "helical screw" mechanism for the four S4 segments of the voltage-sensitive potassium channel (Durrel and Guy, 1992). Without the three-dimensional conformation of these channels, these mechanisms were proposed on the basis of structural models of the channels derived from structure prediction algorithms (Guy and Conti, 1990). At this point, the lack of structural information represents a major difficulty for a detailed understanding of the gating mechanisms of biological channels from a microscopic point of view. Biological channels are known to be broadly divided into those types that are gated through the transmembrane voltage and those that are gated through the binding of chemical messengers (Hille, 1984). The use of such tools as site-directed mutagenesis, from the application of molecular biology to ion channels, has begun to provide insights into the influence of particular amino acids (Bezanilla and Stühmer, 1989; Bezanilla et al., 1991; Sigworth, 1994). Considerable efforts have also been dedicated to a quantitative characterization of the gating dynamics of biological channels in terms of phenomenological kinetic models based on experimental data extracted from single-channel recordings (Auerbach, 1993; Stefani et al., 1994). But, in the absence of tertiary structure, the detailed microscopic movements underlying gating transitions and their relation to kinetic models and site-directed mutations have not been determined.

Traditionally, studies on simple pore-forming molecules have contributed significantly to our understanding of transmembrane ion channels (Hille, 1984). In particular, the ion channel formed by the gramicidin A molecule, a linear antibiotic pentadecapeptide produced by *Bacillus brevis* consisting of alternating L- and D-amino acids, HCO-Val[1]-Gly[2]-Ala[3]-D-Leu[4]-Ala[5]-D-Val[6]-Val[7]-D-Val[8]-Trp[9]-D-Leu[10]-Trp[11]-D-Leu[12]-Trp[13]-D-Leu[14]-Trp[15]-$NHCH_2CH_2OH$, has been the object of numerous experimental (Andersen, 1984; Arseniev et al., 1985; Finkelstein and Andersen, 1981;

Received for publication 20 April 1994 and in final form 19 July 1994.
Address reprint requests to Dr. Benoît Roux, Chemistry Department, Université de Montréal, C. P. 6128, succ. A, Montréal H3C 3J7, Canada. Tel.: 514-343-7105; Fax: 514-343-7586; E-mail: rouxb@ere.umontreal.ca.

0006-3495/94/10/1370/17 $2.00

Nicholson and Cross, 1989; Urry, 1971; Wooley and Wallace, 1992), as well as theoretical (Chiu et al., 1989, 1991; Roux and Karplus, 1993) studies and is probably the most well understood molecular pore (see Roux and Karplus (1994a) and the references therein for a recent review of the theoretical studies). The ion-conducting channel is an N-terminal-to-N-terminal (head-to-head) dimer formed by two single-stranded right-handed $\beta^{6.3}$-helices (Arseniev et al., 1985; Nicholson and Cross, 1989; Urry, 1971), stabilized by the formation of six intermonomer —NH···O— backbone hydrogen bonds. A bimolecular process involving the association and dissociation of the monomers is responsible for the opening and closing of the naturally occurring dimer channel (Hille, 1984). Unimolecular processes such as macromolecular conformational changes are thought to be the dominant mechanism involved in the gating of biological ion channels (Andersen and Koeppe, 1992; Hille, 1984). Chemically modified analogs of the gramicidin channel can provide suitable model systems to study such unimolecular gating processes. One particularly interesting gramicidin channel analog, in which the two monomers were linked at their N-termini with a dioxolane ring, was synthesized by Stankovic et al. (1989). The two stereospecific isomers of the dioxolane-linked gramicidin that were produced, the SS and RR forms, exhibited strikingly different properties. Frequent and rapid interruptions of the current ("flickers") were observed in single-channel recordings with the RR-linked channels but not with the SS-linked channels. In addition, the measured time scale of the interruptions exhibited by the RR-linked channels was similar to that observed in biological channels; the measured blocking rate was 100/s and the average lifetime of blocking was ~0.1 ms. Such flickers, which are not usually observed with channels formed by naturally occurring gramicidin A, were interpreted as evidence for conformational transitions of the dioxolane ring from the outside to the inside of the channel, acting as a gate to block the pore. Similar rapid fluctuations of the channel conductance had been observed previously with *N*-acetyl gramicidin, in which a methyl group is substituted for the N-terminal hydrogen (Seoh and Busath, 1993; Szabo and Urry, 1978). But in the case of this gramicidin analog, it is difficult to separate the dynamics of the gate (here a methylated amide group) from a decrease in the lifetime of the dimer channel.

The microscopic factors involved in the gating properties of the dioxolane-linked channels have not been investigated, and the origin of the differences in behavior between the RR and SS forms is not understood. The two isomers provide a simple molecular model to study gating mechanisms at the microscopic level. Furthermore, the linked channels represent useful systems for studying conformational transitions occurring in proteins. Generally, the individual transition rates of dynamical processes taking place in macromolecules are not easily accessible and only average relaxation times are estimated on the basis of spectroscopic studies (Brooks et al., 1988; Haydock et al., 1990; McCammon and Karplus, 1979; Northrup et al., 1982). In the present case, single-channel recordings allow the detection of the individual transitions of the dioxolane ring. The goal of this paper is to understand the gating of the dioxolane-linked channels at a detailed atomic level by using molecular dynamics simulations. In particular, the microscopic origin of the differences in gating kinetics observed for the two different stereospecific isomers was investigated. The computational approach was similar to that employed in other theoretical investigations of dynamical processes in proteins (Brooks et al., 1988), e.g., the tyrosine ring-flip of BPTI (McCammon and Karplus, 1979; Northrup et al., 1982), the rotational isomerization of tryptophan in scorpion neurotoxin (Haydock et al., 1990), and ion permeation in the gramicidin channel (Roux and Karplus, 1991a, b). Based on the assumption that the general features of the β-helical dimer three-dimensional structure are conserved in the dioxolane-linked channel, a reaction coordinate was defined and the transition rates were calculated using specialized techniques for biased sampling (Berne et al., 1988; Haydock et al., 1990; McCammon and Karplus, 1979; Northrup et al., 1982; Patey and Valeau, 1975; Straub and Berne, 1988; Woolf and Roux, 1994). Computed transition rates were compared with "opening" and "closing" transition rates for the dioxolane-linked channels determined experimentally from single-channel recordings (Stankovic et al., 1989). It was found that the energy barrier for the transition of the dioxolane ring from outside to inside was much bigger for the SS-linked than for the RR-linked form and, furthermore, that the presence of an ion inside the channel strongly stabilized the ring inside conformation and appeared necessary to account for the experimentally observed transition rate in the RR-linked form.

In the following sections, the microscopic model, the potential function, and the computational procedures are described. First, the stable states of the system and the pathway for the gating transition are obtained from an adiabatic potential energy surface. Then, the transition rate constants between the stable states of the system are estimated based on the Smulochowsky-Kramers approximation (Kramers, 1940). This requires the calculation of the potential of mean force (PMF) and the diffusion constant along the reaction coordinate. The main results are discussed and compared with experimentation. The paper concludes with an assessment of the main results and a discussion of the implications for gating in biological channels. Guidelines are given for the future application of the present approach.

METHODS

Microscopic Model and Potential Function

The RR and SS dioxolane-linked gramicidin channels were constructed from the coordinates of the right-handed helical structure of Arseniev et al. (1985). A 1,3-dioxolane ring linker was substituted for the formyl groups at the N-terminus of each gramicidin monomer, with bonds being created to the amino-terminal Val^1 residue. The two stereospecific isomers of the dioxolane linker are shown schematically in Fig. 1. Twelve single-file water molecules were positioned along the axis of the pore, separated by a distance of 2.8 Å; the two central water molecules (the sixth and seventh) enclose the ring when it is inside the pore. The seventh water molecule was replaced

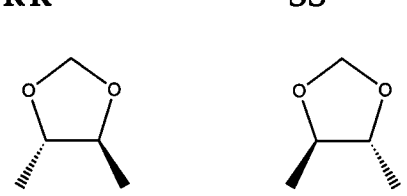

FIGURE 1 Schematic representation of the RR and SS forms of the dioxolane linker. The ring is substituted for the formyl group at the N-terminus of each monomer (see also Fig. 3).

by a K^+ ion in some calculations to examine the influence of a permeating ion on the gating of the dioxolane ring. The channel-channel (CHARMM/XPLOR) (Brooks et al., 1983; Reiher, 1985), water-channel (Reiher, 1985), water-water (TIP3P) (Jorgensen et al., 1983), potential functions used have been described elsewhere. The protein is represented by an extended atom model in which the nonpolar hydrogens are not explicitly included, resulting in a total of 319 atoms in the two model systems. Both the RR and SS dioxolane-linked channels retain the topological symmetry of the head-to-head gramicidin A dimer. The main features of the two linked channels with the dioxolane ring inside and outside the pore are shown in Fig. 2.

The potential function describing the ion-channel interactions includes two modifications to the standard nonbonded energetics: the shortrange core repulsion between the K^+ and the carbonyl oxygen is described with a $\sim 1/r^8$ potential, softer than the Lennard-Jones 6–12 potential, and a first-order polarization term was included for ion-peptide interactions (Roux and Karplus, 1991a, 1994b). Atomic polarizabilities, assigned to all nonhydrogen peptide atoms, were adjusted to reproduce the results from ab initio calculations (Roux and Karplus, 1994b). Their values are similar to other atomic polarizabilities: α is 0.3 for C, 0.5 for methyl groups, 1.5 for N and 1.5 for O. A value of 0.5 is used for the oxygens of the dioxolane ring; no polarizability is assigned to the TIP3P water atoms. The other nonbonded parameters for the dioxolane ring were taken from the OPLS potential (Briggs et al., 1990) and are given in Table 1. A weak half-harmonic confining potential was applied to the oxygen of the three outermost water molecules on each side of the channel to keep them near the entrance of the channel,

$$V_{wat} = \begin{cases} \frac{1}{2}K_{wat}(|\mathbf{R} - \mathbf{R}_0|^2 - R_{max}) & \text{if } |\mathbf{R} - \mathbf{R}_0| \geq R_{max} \\ 0 & \text{otherwise} \end{cases} \quad (1)$$

where R_0 is a reference point located at ± 11 Å along the channel axis. A value of 4 Å was used for R_{max} and a force constant of 1 kcal/mol/Å^2 for K_{wat}.

The nonbonded interactions were calculated on an atom-by-atom basis with a cutoff of 12.0 Å, reduced to 9.0 Å for the computations of the PMF, to save computer time. Shifted electrostatics with a dielectric constant of 1 and van der Waals interactions with a smooth switching function over 1 Å were used. The internal geometry of the TIP3P water molecules and all the bonds involving hydrogen atoms were kept fixed using the SHAKE algorithm (Ryckaert et al., 1977). The center of mass of the dimer was placed at the origin with the channel oriented along the x-axis, the first monomer placed in the $-x$ direction and the second monomer in the $+x$ direction. Most of the trajectories were generated using Langevin dynamics at 300 K with a friction constant corresponding to a relaxation time of 20 ps^{-1} applied to all carbon atoms except those belonging to the dioxolane ring, to ensure a Boltzmann configurational sampling characteristic of the canonical ensemble. An integration time step of 1 fs was used.

TABLE 1 Dioxolane ring parameters

Atoms	ϵ (kcal/mol)	σ (Å)	q (e)
C1, C2	0.080	3.85	0.25
C4	0.118	3.80	0.50
O3, O5	0.170	3.00	−0.50

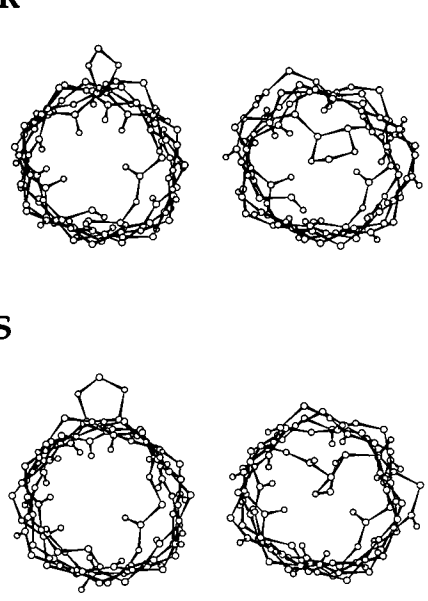

FIGURE 2 View of the RR- and SS-linked gramicidin channels along the pore axis (the side chain atoms are omitted on this figure for the sake of clarity). The open conformation with the ring outside the pore (left) and the closed conformation with the ring inside the pore (right) are shown.

Transition rate theory

The transition rate between two stable states along a free energy curve is given by (Kramers, 1940; Straub and Berne, 1988)

$$k = F_p e^{-\Delta \mathcal{W}^{\ddagger}/k_B T} \quad (2)$$

where $\Delta \mathcal{W}^{\ddagger}$ is the activation free energy barrier and F_p is called the pre-exponential frequency factor. The transition rate is usually dominated by the magnitude of the activation energy, and the influence of the dynamical frequency prefactor is often less important. Although F_p can be calculated exactly using activated dynamics trajectories (Chandler, 1987; Northrup et al., 1982; Roux and Karplus, 1991b), a good estimate may be obtained for the high-friction regime from the Kramers-Smoluchowsky approximation (Straub and Berne, 1988).

$$F_p = \left[\int_{\text{reactant}}^{\text{product}} d\zeta D(\zeta)^{-1} \exp\left(+ \frac{\mathcal{W}(\zeta) - \mathcal{W}(\zeta_b)}{k_B T} \right) \right]^{-1} \times \left[\int_{\text{reactant}} d\zeta \exp\left(- \frac{\mathcal{W}(\zeta) - \mathcal{W}(\zeta_w)}{k_B T} \right) \right]^{-1} \quad (3)$$

An approximate expression can be derived in the case of a high-energy barrier,

$$F_p \simeq \frac{D(\zeta_b)}{2\pi k_B T} [-\mathcal{W}''(\zeta_b)\mathcal{W}''(\zeta_w)]^{1/2} \quad (4)$$

where $D(\zeta_b)$ is the diffusion constant at the barrier top along the reaction coordinate and $\mathcal{W}''(\zeta_b)$ and $\mathcal{W}''(\zeta_w)$ are the second derivatives of the PMF at the barrier and in the reactant well, respectively. In dense systems, where dynamical friction is expected to be significant, Eq. 4 provides an appropriate estimate of F_p (Straub and Berne, 1988). Preliminary tests indicated that the approximation is well justified for the present study (data not shown).

From Eqs. 2 and 4, the evaluation of the transition rate involves the calculation of the PMF $\mathcal{W}(\zeta)$ along a chosen reaction coordinate ζ and an estimate of the diffusion constant $D(\zeta_b)$ at the barrier top. A reaction coordinate involving three transitions was considered in the present investigation. To describe the transition of the dioxolane ring about the C1—C2

bond from outside to inside the channel, the coordinate $q[\mathbf{R}]$ is introduced. It is defined as the cosine between the unit vectors $\hat{\mathbf{u}}$ and $\hat{\mathbf{e}}$, i.e., $q[\mathbf{R}] = \hat{\mathbf{u}} \cdot \hat{\mathbf{e}}$, where $\hat{\mathbf{u}}$ is a unit vector joining the center of mass of the gramicidin dimer to the midpoint between the two C_α of Val[1], and $\hat{\mathbf{e}}$ is a unit vector joining the midpoint between carbons C1 and C2 to carbon C4 (see Fig. 3). Further free-energy calculations were necessary to describe the dihedral torsional transitions along the peptide bond of Val[1]. The choice of reaction coordinate is discussed in more detail in the section reporting the results. Special techniques for sampling with a bias were used to calculate effectively these quantities from a molecular dynamics trajectory (see below). In particular, the PMF was calculated using the "umbrella sampling" technique (Patey and Valeau, 1975), and the diffusion constant was calculated using an analysis based on the Generalized Langevin Equation (Berne et al., 1988; Straub and Berne, 1988). Because the present implementation of these techniques differs slightly from the original applications, they are briefly outlined in the following sections.

$\mathcal{W}(\zeta)$: umbrella sampling technique

To sample the configurational space for the coordinates q and ω-Val[1] ($\equiv \zeta$), the umbrella sampling technique was used (Patey and Valeau, 1975). The PMF, $\mathcal{W}(\zeta)$, is defined from the average distribution function $\langle\rho(\zeta)\rangle$, by

$$\mathcal{W}(\zeta) = \mathcal{W}(\zeta_1) - k_B T \ln\left[\frac{\langle\rho(\zeta)\rangle}{\langle\rho(\zeta_1)\rangle}\right] \tag{5}$$

To enhance the sampling in the neighborhood of a chosen value ζ, the distribution function is calculated from a biased ensemble obtained in the presence of a window potential, $w_i(\zeta)$; a harmonic potential centered on successive values of ζ was used to produce the set of biased ensembles. The biased distribution function obtained from the ith ensemble is

$$\langle\rho(\zeta)\rangle_{(i)} = e^{-\beta w_i(\zeta)}\langle\rho(\zeta)\rangle\langle e^{-\beta w_i(\zeta)}\rangle^{-1} \tag{6}$$

The unbiased PMF from the ith window is

$$\mathcal{W}_i(\zeta) = -k_B T \ln[\langle\rho(\zeta)\rangle_{(i)}] - w_i(\zeta) + \mathcal{C}_i \tag{7}$$

where the undetermined constant, $\mathcal{C}_i$, is equal to $k_B T \ln[\langle e^{-\beta w_i(\zeta)}\rangle]$. In combining the results from different windows it is only necessary to determine the relative value of the constants, i.e.,

$$\mathcal{C}_i = [\mathcal{C}_i - \mathcal{C}_{i-1}] + \cdots + [\mathcal{C}_3 - \mathcal{C}_2] + [\mathcal{C}_2 - \mathcal{C}_1] + \mathcal{C}_1 \tag{8}$$

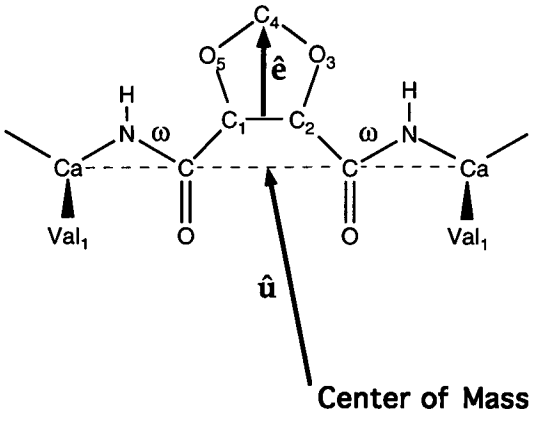

FIGURE 3 Schematic representation of the 1,3-dioxolane ring covalently linked to the amino terminal Val[1] residues of each gramicidin monomer. The two unit vectors $\hat{\mathbf{u}}$ and $\hat{\mathbf{e}}$, used to define the coordinate q ($q[\mathbf{R}] = (\hat{\mathbf{u}}\cdot\hat{\mathbf{e}})$) and the peptide bond dihedral angle ω between the dioxolane and Val[1], are also shown. The vector $\hat{\mathbf{u}}$ joins the center of mass of the gramicidin dimer to the midpoint between the two C_α of Val[1] and the $\hat{\mathbf{e}}$ joins the midpoint between carbon C1 and C2 to carbon C4.

where $[\mathcal{C}_i - \mathcal{C}_j]$ is the free-energy difference between the ith and jth window potentials (Haydock et al., 1990; Woolf and Roux, 1994)

$$[\mathcal{C}_i - \mathcal{C}_j] = -k_B T \ln[\langle\exp(-\beta[w_i(\zeta) - w_j(\zeta)])\rangle_{(j)}] \tag{9}$$

leaving only one arbitrary constant, $\mathcal{C}_1$, to be determined from ζ_0 and $\mathcal{W}_0$ in Eq. 5.

To obtain the final unbiased estimate of the PMF, $\mathcal{W}(\zeta)$, the estimates from the different windows, $\mathcal{W}_i(\zeta)$, are combined by a weighted average proportional to their relative occurrence in the biased distribution function, i.e. (Woolf and Roux, 1994),

$$\mathcal{W}(\zeta) = \sum_i \mathcal{W}_i(\zeta)\frac{\langle\rho(\zeta)\rangle_{(i)}}{\sum_j\langle\rho(\zeta)\rangle_{(j)}} \tag{10}$$

Eq. 10 results in a smooth function $\mathcal{W}(\zeta)$ over the whole range of ζ, giving more weight to the estimate of the ith window where the biased distribution, $\langle\rho(\zeta)\rangle_{(i)}$, is more important. The present procedure to unbias and assemble the different windows, Eq. 10 in particular, differs from the original umbrella sampling method described by Patey and Valeau (1975).

$D(\zeta_b)$: generalized Langevin equation technique

The value of the diffusion constant close to the transition state along the reaction coordinate, $D(\zeta_b)$, is needed for the evaluation of the transition rate and the time scale of the dynamics of the reaction coordinate, (see Eqs. 2 and 4). To extract the local diffusion constant at any particular location, ζ_i, along a reaction coordinate, a general technique was proposed by Straub and Berne (Berne et al., 1988; Straub and Berne, 1988). The technique is based on an analysis in terms of a generalized Langevin equation,

$$\frac{k_B T}{\langle\dot{\zeta}^2\rangle_{(i)}}\dot{C}(t;\zeta_i) = -\frac{k_B T}{\langle\delta\zeta^2\rangle_{(i)}}\int_0^t C(t';\zeta_i)\,dt' - \int_0^t M(t-t';\zeta_i)C(t';\zeta_i)\,dt' \tag{11}$$

where $M(t;\zeta_i)$ and $C(t;\zeta_i)$ are the ζ-dependent memory function and the time correlation function of the velocity, $\dot{\zeta}$, $\delta\zeta$ represents the deviation of ζ from its average, $\delta\zeta = \zeta(t) - \langle\zeta\rangle_{(i)}$. In Eq. 11, all averages, $\langle\cdots\rangle_{(i)}$, are performed in the presence of a biasing harmonic window potential.

The diffusion constant at ζ_i is related to the $s \to 0$ limit of the Laplace transform of the memory function,

$$\hat{M}(s;\zeta_i) = \int_0^\infty e^{-st}M(t;\zeta_i)\,dt \tag{12}$$

through Einstein's relation

$$D\zeta_i) = \lim_{s\to 0}\frac{k_B T}{\hat{M}(s;\zeta_i)}. \tag{13}$$

The latter yields, after some algebra (Woolf and Roux, 1994),

$$D(\zeta_i) = \lim_{s\to 0}\frac{-\hat{C}(s;Z_i)\langle\delta\zeta^2\rangle_{(i)}\langle\dot{\zeta}^2\rangle_{(i)}}{\hat{C}(s;\zeta_i)[s\langle\delta\zeta^2\rangle_{(i)} + \langle\delta\dot{\zeta}^2\rangle_{(i)}/s] - \langle\delta\zeta^2\rangle_{(i)}\langle\delta\dot{\zeta}^2\rangle} \tag{14}$$

This formalism follows from the generalized Langevin equation for a harmonic oscillator. It is based on the assumption that the motional variations of ζ_i are restricted to the neighborhood of ζ_b by the window potential.

Simulation procedure for PMF and diffusion constants calculations

The PMF describing the transitions along each of the paths Out-*trans* to Out-*cis* (ω-Val[1] varies from 180 to 0° while $q \approx +1$), Out-*cis* to In-*cis* (q varies from +1 to −1 while $\omega \approx 0$), In-*cis* to In-*trans* (ω varies from 0 to 180° while $q \approx -1$), and Out-*trans* to In-*trans* (q varies from +1 to −1 while $\omega \approx 180$) were calculated for the SS- and RR-linked forms using the

umbrella sampling technique. In the following, the calculated PMFs along these paths are referred to as $\mathcal{W}_{out}(\omega)$ (Out-*trans* to Out-*cis*), $\mathcal{W}_{cis}(q)$ (Out-*cis* to In-*cis*), $\mathcal{W}_{in}(\omega)$ (In-*trans* to In-*cis*), and $\mathcal{W}_{trans}(q)$ (Out-*trans* to In-*trans*). To examine the symmetry of the PMF along the ω dihedral, the PMF along the path Out-*trans* to Out-*cis* was also calculated for ω varying from -100 to 320° for the SS-linked form.

The PMF along a given path was calculated from several trajectories generated in the presence of a harmonic window potential applied to one value of the reaction coordinate, whereas the other coordinate was restricted in the appropriate subset of configurational space. For example, the PMF $W_{in}(\omega)$ along the path In-*cis* to In-*trans* was calculated by generating several trajectories in the presence of a harmonic dihedral potential centered on successive values of the dihedral angle ω, while a repulsive half-harmonic restraint (active only if $q \geq 0$) was applied to the coordinate q to prevent an unwanted transition of the dioxolane ring to the "Out" state during the calculations (all other degrees of freedom were unrestrained). In practice, such half-harmonic restraints were unnecessary for the PMF calculations along the coordinate q because a large barrier prevented unwanted spontaneous transitions of the peptide bond dihedral angle. The total number of windows and the force constant of each window potential were both adjusted to obtain good convergence. Typical values of the force constant were 50 kcal/mol/radian^2 for the PMF along coordinate ω and 200 kcal/mol/$[q]^2$ for those along coordinate q; ~15–20 windows were generated and combined using Eq. 10. Careful checking was done to make sure that there was sufficient overlap between the biased histograms. For each window, the configurational sampling was generated from a 50-ps trajectory of Langevin dynamics in the presence of the window potential; the initial configurations were equilibrated with several cycles of simulated annealing with Langevin dynamics and energy minimization starting from the last configuration of the previous window. Special care was taken to equilibrate the initial configuration used for the umbrella sampling calculations. During the early stage of equilibration, various energy restraints were used to maintain the conformation of the linked dimer channel. The C_α from the Val^1 residues were restrained to a reference position with an initial force constant of 5.0 kcal/mol, other atoms in the gramicidin channel were restrained with a force constant of 1.0 kcal/mol, and atoms from the dioxolane ring were unrestrained. The distance between the water oxygens of nearest neighbors in the single file were restrained to a maximum of 2.8 Å using harmonic potentials. At the end of the equilibration period, the restraints were progressively reduced down to 0 in 10 ps, and the structure was equilibrated for an additional 5 ps.

The diffusion constants were calculated from trajectories of 100 ps generated with harmonic biasing window potentials to restrain the reaction coordinate to be near the barrier top in a similar manner to the restraints used in the PMF calculations. The diffusion constants were calculated from the Laplace transform of the velocity autocorrelation functions using Eq. 4. The velocity autocorrelation functions were integrated numerically using the trapezoidal rule to calculate the Laplace transform. Because the Laplace transform is singular for $s \rightarrow 0$ in Eq. 14, the values were extrapolated by least-squares fitting a straight line at small values of s.

The transition rates were calculated using Eq. 2. The preexponential frequency factor was evaluated numerically with Eq. 3 using an explicit integration based on the trapezoidal rule. The approximate expression Eq. 4 was also evaluated; the second derivatives of the PMF at the barrier W''_b and in the reactant well W''_w, used in Eq. 4, were calculated by least-squares fitting a parabola to $W(\xi)$.

Protocol for adiabatic energy maps

Two-dimensional adiabatic potential energy surfaces, $U_{adia}(q, \omega)$, were computed as a function of q and ω-Val^1 for both SS- and RR-linked channels in the absence of water molecules. The adiabatic energy surface $U_{adia}(q, \omega)$ corresponds to the minimum potential energy of the dioxolane ring-linked channel for prescribed values of the variables q and ω of Val^1 (i.e., the geometry is optimized with respect to all coordinates other than q and ω). The adiabatic surfaces for the SS- and RR-linked channels were calculated for each point of a 21×20 grid with q varying from -1.0 to $+1.0$ in steps of 0.1 and ω varying from 0.0 to 190.0° in steps of 10.0°.

A special protocol was used to calculate the adiabatic energy surface. First, a configuration was taken from a relaxed geometry of the dioxolane ring-linked channel; an initial channel structure with ω of Val^1 in the *trans* state was used for the upper half of the adiabatic surface ($\omega > 0°$) and an initial channel structure with ω in the *cis* state was used for the lower half ($\omega < 0°$). The upper and lower halves of the surface were calculated from different initial configurations, because attempts to calculate the adiabatic surface for ω varying from 0 to 190° directly exhibited large discontinuities for values of q near 0 because of the existence of multiple minima. Second, the initial configuration was refined in the presence of strong harmonic energy restraints to maintain the value of $q[R]$ near a prescribed value using several cycles of simulated annealing with restrained Langevin dynamics and energy minimization. During the annealing period, the NOE restraint potential of XPLOR was used with a force constant of 2 kcal/mol/Å^2 to maintain the hydrogen bonds of the β-helix dimer; the four hydrogen bonds closest to the ring were not restrained. Third, the resulting configuration was refined in the presence of a strong harmonic restraint to maintain the values of both $q[\mathbf{R}]$ and $\omega[\mathbf{R}]$ near prescribed values using a similar protocol of simulated annealing and energy minimization. The q reaction coordinate force constant was 5000 kcal/$[q]^2$; the ω-dihedral was restrained with a force constant of 1000 kcal/(mol rad^2). The contribution of the harmonic restraints was not included in the final energy. In all cases, the simulated annealing trajectories were generated with Langevin dynamics, and the energy minimization was carried out using the Powell algorithm.

RESULTS AND DISCUSSION

Choice of the reaction coordinate

During preliminary studies (Crouzy et al., 1992) the gating transition of the dioxolane ring was described by the coordinate $q[\mathbf{R}]$ (see Fig. 3). At this early stage, the function $q[\mathbf{R}]$ seemed to represent an appropriate reaction coordinate to describe the gating transition: its value changes from $+1$ to -1 when the ring moves from outside to inside the channel. However, attempts to calculate the PMF exclusively on the basis of $q[\mathbf{R}]$ were unsuccessful (Crouzy et al., 1992). In particular, spontaneous isomerizations of the dioxolane-Val^1 peptide bond from the initial *trans* configuration to a *cis* configuration were sometimes observed during the trajectories that were generated to calculate the PMF along the coordinate q (Crouzy et al., 1992). The calculated PMFs were thus statistically poor because the conformational sampling of the configurations assumed by the peptide bond was inaccurate because of a significant torsional energy barrier (Brooks et al., 1983). Generally, such difficulties in a PMF are an indication that the chosen reaction coordinate is not sufficient to provide a complete description of the dynamical transition in the system (G. Ciccotti, personal communication). It was thus apparent that both q and the peptide bond dihedral angle ω of Val^1 were involved in the gating transition, and the variable q alone could not describe completely the dynamics of the dioxolane ring. Ideally, the correlations between the coordinates q and ω of Val^1 would be best studied by calculating the two-dimensional PMF as a function of both variables. Because such computations are far too expensive, adiabatic energy surfaces were calculated as a function of q and ω to first gain information about the dominant potential energy barriers controlling the conformational transitions in the system. The calculated adiabatic surfaces for both the SS- and RR-linked channels are shown in Fig. 4, and information about the local minima is summarized in

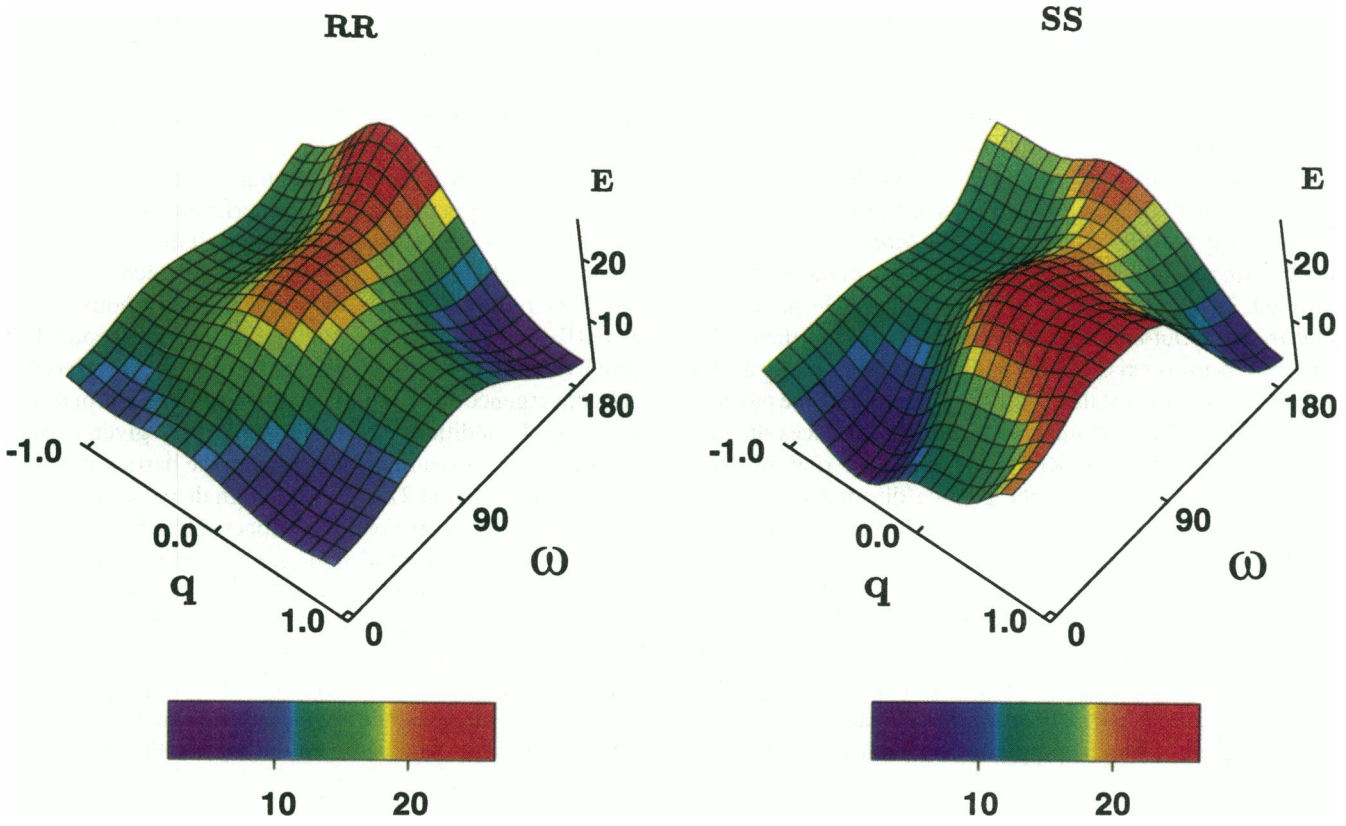

FIGURE 4 Adiabatic energy surface calculated as a function of the q and ω-Val[1] coordinates for the SS and RR forms. The minimum energy of each surface has been set to 0 for display. Red colors refer to high energies and correspond to forbidden regions on the surface. For the RR-linked form, an energetically favorable pathway going through the four states can be observed: $\omega \approx 180$ and $q \approx +1$ (ring outside and dihedral angle in the *trans* conformation), $\omega \approx 0$ and $q \approx +1$ (ring outside and dihedral angle in the *cis* conformation), $\omega \approx 0$ and $q \approx -1$ (ring inside and dihedral angle in the *cis* conformation) and finally, $\omega \approx 180$ and $q \approx -1$ (ring inside and dihedral angle in the *trans* conformation). In contrast, no energetically favorable pathway leaving the region corresponding to $\omega \approx 180$ and $q \approx +1$ (ring outside and dihedral angle in the *trans* conformation) is observed for the SS-linked form.

Table 2. Difficulties in the calculation of the adiabatic surface are related to the existence of multiple minima in the potential energy of the system (McCammon and Karplus, 1979). Because configurations can get trapped in local minima during geometry optimization, calculated surfaces can exhibit various discontinuities and defects. To avoid such multiple-minima problems, the surfaces were calculated with no water molecules using a special protocol (see the description in the previous section). Despite the special care taken to optimize the geometries, difficulties due to multiple minima were observed for a few critical values (for q near 0 and ω near 90°), and the calculated surface became discontinuous. The discontinuities were smoothed by combining the values of both halves, calculated from initial *cis* and *trans* structures, over an interval of 50° around values of ω close to 90°, and through averaging by energetic weight the calculated total energies. For this reason, the calculations do not correspond to the lowest minimum in energy and the results are not true adiabatic energy surfaces. Nevertheless, the results are qualitatively meaningful and provide much insight into the possible paths for the gating transition of the dioxolane ring from inside to outside the channel.

Observation of the adiabatic surfaces indicated that the Out-*trans* state corresponds to low-energy minimum for

TABLE 2 Minima of the adiabatic energy surface*

States	RR-linked form			SS-linked form		
	ω (degrees)	q	Energy (kcal/mol)	ω (degrees)	q	Energy (kcal/mol)
Out-*trans*	199	0.99	0.0	183	0.98	0.0
Out-*cis*	13	0.74	6.7	10	0.50	8.3
In-*cis*	11	−0.73	8.8	14	−0.43	−0.7
In-*trans*‡	132	−0.69	10.9	144	−0.63	10.1
	136	−0.92	12.9			

* All energies are given relative to the Out-*trans* state. ‡ The second line refers to a substate of the In-*trans* conformation.

the SS- and RR-linked channels. The Out-*cis*, In-*cis*, and In-*trans* states correspond to energy minima on the adiabatic surface with the In-*trans* state having the highest energy, although the energy well of the Out-*cis* state is very shallow in the SS-linked case. The Out-*trans* represents the absolute minimum in the RR-linked case, whereas the In-*trans* state is lower by 0.7 kcal/mol in the SS-linked case (see Table 2). High-energy barriers separate the Out-*trans* state from both the In-*trans* and the Out-*cis* states in the case of the SS-linked channel. In contrast, an energetically favorable path from Out-*trans* to Out-*cis*, from Out-*cis* to In-*cis*, and then from In-*cis* to In-*trans* exists for the RR channel, suggesting a path for rapid transitions of the dioxolane ring to block the passage of ions. Thus, the adiabatic potential energy surfaces showed that the transition of the RR-linked dioxolane ring must involve the isomerization of the peptide dihedral angle ω of Val^1. The transition of the dioxolane-linked gramicidin channel from an "unblocked" to a "blocked" state can be described by a three-step reaction: Out-*trans* $\rightarrow$ Out-*cis* $\rightarrow$ In-*cis* $\rightarrow$ In-*trans* (the four stable states involved in the transition of the RR-linked form are illustrated in Fig. 5). In fact, several equivalent pathways are possible due to the symmetry of the system (n.b., although the two dioxolane-linked channels have different properties, in both cases their topology possesses the C_2 symmetry axis of the head-to-head gramicidin A dimer). For example, the *cis-trans* isomerization of the peptide bond of Val^1 on either one of the two monomers can initiate the transition of the dioxolane ring toward the inside of the channel. The ring turns toward the first monomer when the dihedral angle ω of Val^1 of the first monomer undergoes a *trans-cis* isomerization (by symmetry, the ring will turn in the opposite direction if the isomerization occurs at Val^1 of the second monomer). Such symmetry should be reflected in the statistical averages of both the SS- and RR-linked forms, i.e., the results are independent of which monomer is chosen, although it can be expected that the convergence may require an extensive conformational sampling. In addition, the isomerization of a given peptide bond can occur via a transition through the barrier at 90°, or through the barrier at 270°. Even though these two pathways are not formally equivalent, it is expected that the activation energies for the ω dihedral angle are very similar. To further extend the information provided by the adiabatic surfaces (calculated with the channel in vacuum), the stable conformations of the system were characterized with molecular dynamics simulations of the dioxolane-linked channels in the presence of single-file water molecules and the transition rate between the four stable states Out-

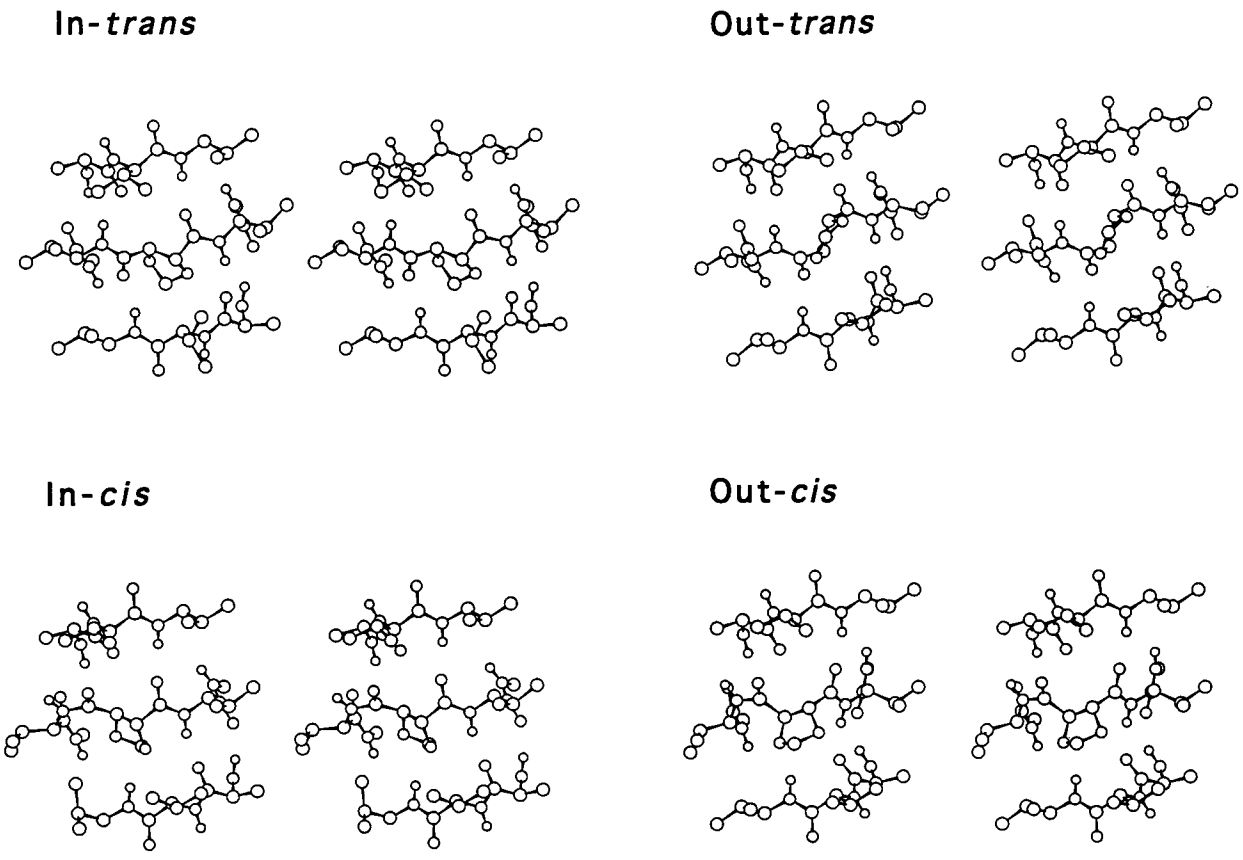

FIGURE 5 Stereo representation of the reaction in three steps describing the gating transition of the RR-linked dioxolane ring from outside to inside the channel. The four states Out-*trans*, Out-*cis*, In-*trans*, and In-*cis* are shown (the spatial arrangement of the four states corresponds to that of the adiabatic energy surface in Fig. 4). In all the figures, the first monomer is at the bottom (starting on the left of the dioxolane ring) and the *x*-axis is pointing upward. The dihedral angle ω-Val^1 of the first monomer undergoes an isomerization (located on the left of the dioxolane ring).

trans, Out-*cis*, Inside-*cis*, and Inside-*trans*, were calculated. The results of these calculations are described in the following sections.

Characterization of the stable states

Each of the four stable states for the SS- and RR-linked forms was characterized by generating 100-ps trajectories of Langevin dynamics at 300 K with 12 single-file water molecules. Preliminary studies indicated that the hydrogen bonds of the β-helical structure appeared to be less stable during simulations of the isolated channel in vacuum, whereas they remained stable during all the simulations when single-file waters were included. The initial structures, taken from the corresponding energy minima found on the adiabatic energy surfaces, were refined with several cycles of simulated annealing with restrained Langevin dynamics and with energy minimization to equilibrate the single-file waters and the dioxolane ring. Fig. 6 shows two-dimensional histograms of the SS and RR conformations in their equilibrium states averaged over 100-ps molecular dynamics trajectories. More information about the q and ω coordinates and the dioxolane ring puckering (Cremer and Pople, 1975) is given in Table 3.

Overall, the average values of the q and ω coordinates are in good accord with the optimized configurations of Table 2, although there are some differences. In particular, the average value of q is shifted toward -1 (i.e., the ring is pushed inward) relative to the position of the energy minimum on the adiabatic surface for the In-*trans* state (see Tables 2 and 3). Moreover, the average value of q is shifted toward 0 (i.e., the ring is pushed outward) relative to the position of the energy minimum on the adiabatic surface for the In-*cis* state of the RR-linked channel (the average is -0.31 in Table 3, whereas the position of the minimum is at -0.7 in Table 2). Vacuum simulations of the channel in the In-*cis* and In-*trans* conformations were performed to examine the role of the single-file water molecules on the stability of the dioxolane ring inside the channel in the case of the RR-linked form. The results are also given in Table 3. The average of q calculated from the vacuum simulations of the In-*cis* and In-*trans* states are in closer agreement with the position of the energy minima on the adiabatic surface than the averages calculated with single-file waters. In addition, the fluctuations of the ring pucker for the In-*trans* state appear to be considerably reduced in the presence of single-file waters. During the vacuum simulation of the RR form in the In-*trans* state, brief concerted transitions were observed in which q varied from -0.69 to -0.95 and ω from 130 to 150°. The transitions were correlated with variations of the second pucker value from 110 to 300°. These correlated fluctuations are in accord with the adiabatic surface, where two shallow wells separated by a small barrier of 2 kcal/mol exist for the state In-*trans* (see Table 2). With no waters inside the channel, the ring fluctuates between the two wells, whereas it is stabilized in the well corresponding to $q = -0.95$ in the presence of waters.

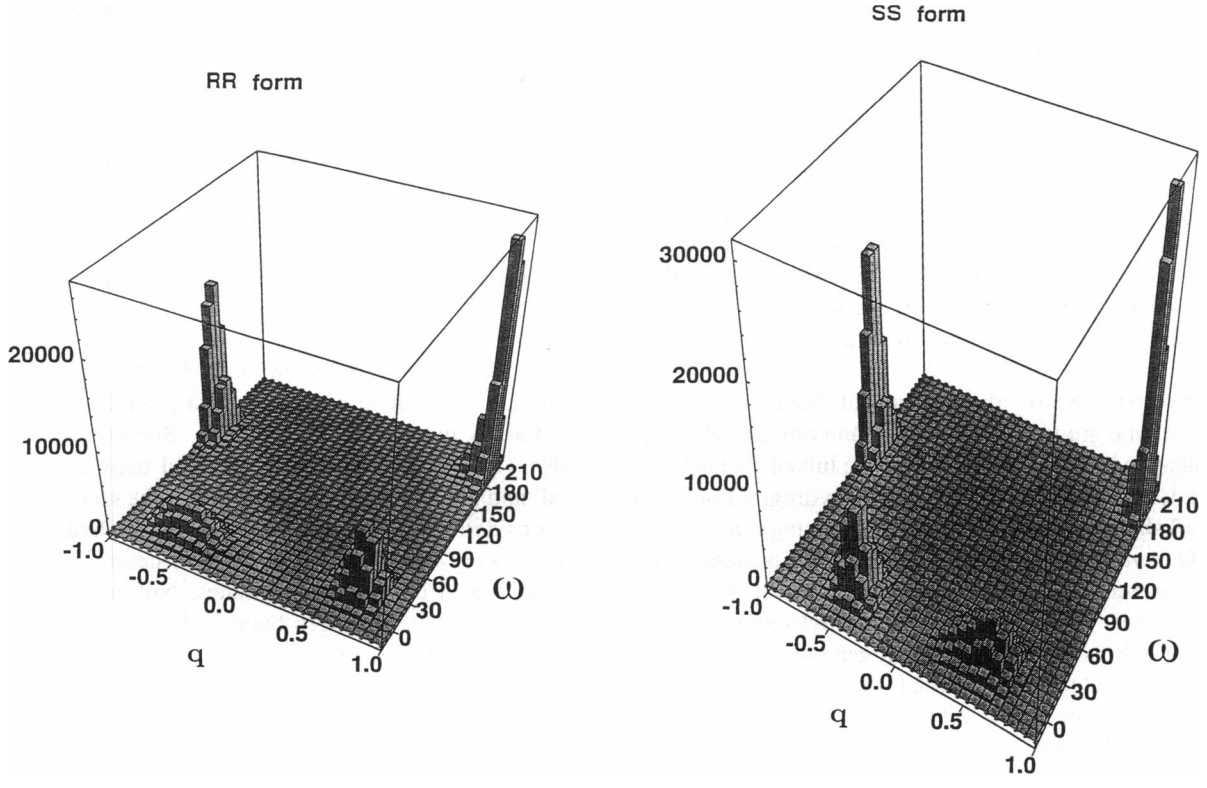

FIGURE 6 Probability histograms of the RR and SS forms of the dioxolane-linked channel in the four stable states. The histograms were obtained from four independent dynamics runs of 100 ps, and the relative weighting of each state does not reflect the absolute populations of the states.

TABLE 3 Average structural properties of the stable states

States	RR-linked form ω (degrees)	RR-linked form q	RR-linked form Pucker (degrees)	SS-linked form ω (degrees)	SS-linked form q	SS-linked form Pucker (degrees)
Out-*trans*	191 (8)	0.95 (0.05)	213 (49)	188 (7)	0.96 (0.03)	−5 (54)
Out-*cis*	20 (10)	0.70 (0.09)	142 (15)	14 (10)	0.51 (0.13)	360 (37)
In-*cis**	13 (9)	−0.31 (0.22)	266 (12)	15 (9)	−0.45 (0.08)	326 (32)
	15 (11)	−0.68 (0.08)	269 (17)			
In-*trans**	133 (10)	−0.95 (0.03)	294 (15)	132 (10)	−0.96 (0.03)	303 (17)
	132 (13)	−0.69 (0.12)	97 (39)			

The rms fluctuations are given in parenthesis. * The second line was calculated from simulations with no single-file water molecules.

In contrast, the presence of waters inside the channel tends to "push" the ring outside the channel when it is in the state In-*cis* (the average value of q increases from −0.69 to −0.32). These observations suggest that the interactions of the dioxolane ring with the water inside the channel are responsible for the difference and that the presence of the single-file water molecules results in a stabilization of the In-*trans* state, and in a destabilization of the In-*cis* state.

Based on the adiabatic energy surface, the configuration with the dioxolane ring outside and the peptide bond of Val^1 in the *trans* conformation are energetically very stable in the case of both the RR and the SS forms. The stability of this configuration is reflected in the relatively small fluctuations of q and ω. Despite the dynamical stability of the full system at this configuration, the variation of the internal geometry of the ring appears to have larger fluctuations when it is outside the channel; e.g., the rms of the second pucker values are noticeably larger in the Out-*trans* state. Analysis of the fluctuations shows that this is due to the fact that the ring alternates between two pucker values (150 and 250° for RR and −40 and 80° for SS). Some correlation was observed between the coordinate q and the value of the ring puckering. This is not surprising, given that they both depend on the position of ring carbon C4 (see Fig. 3). Interactions with the hydrocarbon chains of the phospholipid membrane, ignored in the present study, could influence the fluctuations of the dioxolane ring in the Out-*trans* and Out-*cis* states (see also the comparison with experimental results below).

The hydrogen bonds of the β-helical dimer structure involving atomic groups near the dioxolane ring are perturbed by the change in the conformation of the linked channel. The average length of a few characteristic hydrogen bonds are given in Table 4 (see also Fig. 3). When the ring is in the most stable Out-*trans* state, the hydrogen bonds present in the system are very similar to those in the natural gramicidin dimer channel. For example, the carbonyl oxygen groups flanking the dioxolane ring are hydrogen bonding to the NH group of Val^7 (substituting for the formyl groups of the natural gramicidin dimer). It should be noted that the hydrogen bonds in the RR-linked channel are slightly longer than those in the SS-linked channel, suggesting that the dioxolane ring represents a smaller perturbation on the β-helical dimer structure when it is linked in the SS form than in the RR form.

TABLE 4 Hydrogen bonding distances (Å)

Hydrogen bond*	States	RR-linked form	SS-linked form
Val^7—NH···O=C—Diox	Out-*trans*	2.0	2.0
	Out-*cis*	5.9	6.6
	In-*cis*	5.9	4.6
	In-*trans*	2.1	2.0
Val^7—NH′···O=C—Diox′	Out-*trans*	2.0	2.0
	Out-*cis*	2.0	2.2
	In-*cis*	2.1	2.1
	In-*trans*	2.1	2.0
Val^1—NH···O=C—$Ala^{5'}$	Out-*trans*	2.1	2.0
	Out-*cis*	2.8	2.9
	In-*cis*	3.3	3.1
	In-*trans*	1.9	1.9
Val^1—NH′···O=C—Ala^5	Out-*trans*	2.1	2.0
	Out-*cis*	2.2	2.1
	In-*cis*	2.3	2.0
	In-*trans*	2.0	1.9
Ala^5—NH′···O=C—Val^1	Out-*trans*	2.0	2.0
	Out-*cis*	2.1	2.1
	In-*cis*	2.1	2.0
	In-*trans*	2.2	2.1
Gly^2—NH···O=C—Val^7	Out-*trans*	2.0	2.0
	Out-*cis*	2.2	2.0
	In-*cis*	2.7	2.1
	In-*trans*	2.0	2.0
H_2O···H_2O‡	Out-*trans*	2.8	2.8
	Out-*cis*	2.7	2.8
	In-*cis*	3.8	8.6
	In-*trans*	6.9	7.4

* The prime indicates the second GA monomer.
‡ Distance between the oxygens of the two central single-file waters.

The hydrogen bond between the NH of Val^7 and the C=O carbonyl of the dioxolane ring is lost when the peptide bond of Val^1 is in the *cis* conformation. Simultaneously, Val^1-NH···O′=C-Ala^5, the hydrogen bond between the NH of Val^1 and the C=O carbonyl of Ala^5 of the second monomer is considerably weakened. Nevertheless, the hydrogen bonding network of the β-helical dimer structure is remarkably conserved in the four stable states. Not surprisingly, it is observed that the hydrogen-bonded chain of waters is broken when the ring is inside the channel. In the case of the SS-linked form, the average distance between the central waters is larger in both the In-*cis* and In-*trans* states, which suggests that the hydrogen-bonded chain is broken during the transition from the Out-*cis* state to the In-*cis* state. The case of the RR-linked form appears to be more complicated. In the In-*cis* state, the average distance between the central waters

is only 3.8 Å, indicating that the hydrogen-bonded chain can form. However, there are large fluctuations in the oxygen-oxygen distance (±1 Å), suggesting that the hydrogen-bonded water chain is perturbed by the ring when it is in this state. The tendency of the central single-file water molecules to hydrogen bond to one another results in a net force pushing the dioxolane ring outside the channel, which destabilizes the In-*cis* state toward the Out-*cis* state (i.e., toward positive values of q; see Table 3). The stable states found for the RR-linked form from the adiabatic energy surface indicate that values of q shifted toward 0 occur in going from the state In-*trans* to the state In-*cis*. Examination of the three-dimensional structure of the channel showed that the fluctuations in the hydrogen bonds and the motions of the ring were correlated because of variations in the inclination of the plane of the ring with respect to the x-axis. For values of q equal to -0.7, the inclination of the ring was 45°, the hydrogen-bonded chain was broken, and the ring was well inside the channel, making an angle of 45° with respect to the x-axis. For values of q closer to -0.4, the inclination was close to 20° and the ring was pushed outside the channel, allowing the reconstruction of a hydrogen-bonded line of waters. During the transition from Out-*cis* to In-*cis*, the rotation of the ring from outside to inside the channel was accompanied by a change in the mean second pucker value from about 130 to 260°. It follows that correlated motions of the ring and of the two central waters in the hydrogen-bonded chain must take place during the transition from the state Out-*cis* to the state In-*trans*. In the gramicidin A channel, it is known that such movements of the single-file waters in the gramicidin A channel are highly correlated and are sensitive to the the flexibility of the backbone (Chiu et al., 1989; Chiu et al., 1991). Although this concerted process might be better described by a more sophisticated reaction coordinate, further analysis indicates that the observed blocking rate and the average lifetime of block are determined by the slower events involving the *cis-trans* isomerization of the peptide bond (see the following sections).

Transition rate calculations

All information concerning the rate constants (activation energies, diffusion constants, and preexponential frequency factors) are summarized in Table 6. The transition rates were calculated from the PMF and the diffusion constants from Eqs. 2, 4, and 14. The PMFs were calculated along the q and ω reaction coordinates for both the RR and SS forms in the presence of 12 single-file water molecules using Eq. 10. The results are shown in Figs. 7 and 8. The diffusion constants were calculated following the same simulation procedure using the Laplace transform of the reaction coordinates velocity autocorrelation function at the barrier top in Eq. 14. The results are given in Table 5.

The PMF for the gating transition of the SS form is shown as the three-step reaction Out-*trans* → Out-*cis* → In-*cis* → In-*trans* in Fig. 7. Also included is the PMF corresponding to a direct transition from Out-*trans* to In-*trans*. The direct pathway appears to be more energetically favorable (the barriers are 31 kcal/mol for the Out-*trans* to Out-*cis* transition and 21 kcal/mol for the Out-*trans* to In-*trans* transition), although the activation free energy barriers are significant in both cases. The sharp barrier observed for a value of q near -0.1 in the PMF $W_{trans}(q)$, calculated for the transition from Out-*trans* to In-*trans*, corresponds to a change in the hydrogen bonded structure of the single-file water molecules during the insertion of the ring inside the channel (a similar rearrangement of the hydrogen-bonded chain takes place during the step from In-*cis* to Out-*cis*).

The PMF for the gating transition of the RR form is shown with the same three-step reaction Out-*trans* → Out-*cis* → In-*cis* → In-*trans* in Fig. 8. Several difficulties arose in attempts to estimate the transition rate constants for the RR form. In accord with the 100-ps equilibrium trajectory, which indicated that the ring is not very stable inside the channel in the presence of water molecules (see Table 3), the state In-*cis* corresponds to a very shallow energy well in the PMF $W_{cis}(q)$. Because they represent unstable states, the transition rates between the Out-*cis* and In-*cis* states are not meaningful and are not reported in Table 6. Furthermore, early attempts to calculate the PMF $W_{trans}(q)$ for the RR form along the direct path from Out-*trans* to In-*trans*, as was presented for the SS form, were unsuccessful because the β-helical dimer structure was disrupted near the very unfavorable configurations around $q \approx 0$ and $\omega \approx 180$ (Crouzy et al., 1992). Based on the adiabatic energy surface, this pathway appears to be less energetically favorable relative to the three-step process described above, indicating that the dynamics of the dioxolane ring are not determined by such a mechanism.

The magnitude of the transition rate constant is dominated by the exponential Boltzmann factor. Interestingly, the preexponential factor is around 10^{12}/ps in each case, on the same order as the value from gas phase classical transition state theory (Glasstone et al., 1941), k_BT/h, which is often erroneously used in applications to dense systems (Läuger, 1973). However, in the present case the preexponential factors were calculated from the diffusion constants of the curvilinear reaction coordinate functions $\zeta[\mathbf{R}]$ (i.e., $q[\mathbf{R}]$ and $\omega[\mathbf{R}]$) at the barrier top using the velocity autocorrelation function Eq. 14. The magnitude of the diffusion constants $D(q_b)$ and $D(\omega_b)$ calculated using Eq. 14 may be understood from a simple argument. Assuming that for a short time t, the motions of the reaction coordinate ζ obey a simple diffusive process,

$$\langle \Delta\zeta(t)^2 \rangle_{(i)} = 2D(\zeta_i)t \tag{15}$$

For small displacements,

$$\Delta\zeta[\mathbf{R}(t)] \simeq \sum \Delta R_n(t) \frac{\partial \zeta[\mathbf{R}]}{\partial R_n} \tag{16}$$

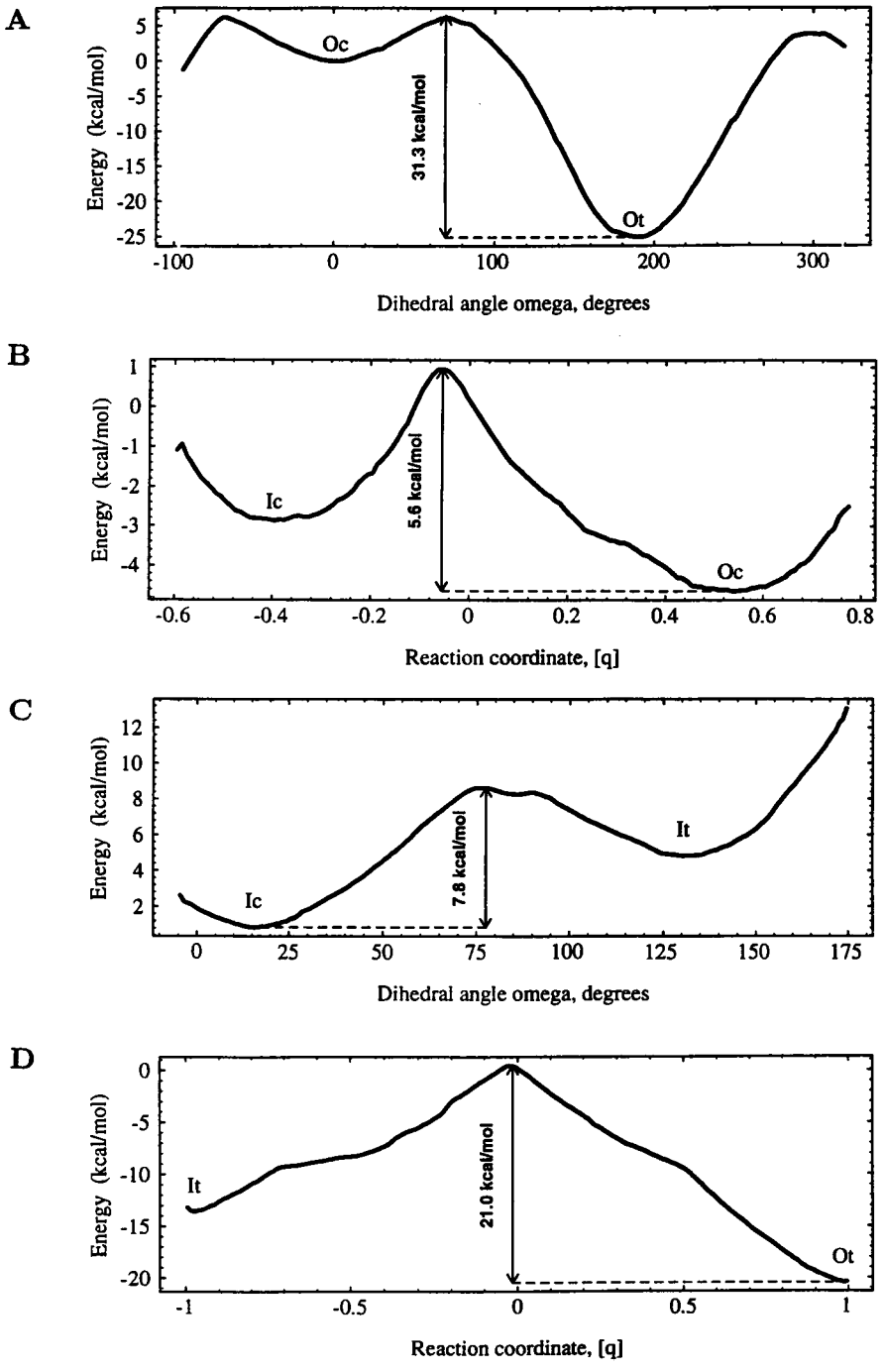

FIGURE 7 PMF along the two pathways for the gating transition of the SS-linked form from outside to inside the channel. The PMF $W_{out}(\omega)$ (*A*), $W_{cis}(q)$ (*B*), and $W_{in}(\omega)$ (*C*) for the three-step reaction Out-*trans* to Out-*cis*, Out-*cis* to In-*cis*, In-*cis* to In-*trans* and the PMF $W_{trans}(q)$ for the direct transition Out-*trans* to In-*trans* (*D*) are shown.

such that, on average,

$$\langle \Delta\zeta(t)^2 \rangle_{(i)} \simeq \sum_{mn} \left\langle \Delta R_m(t) \Delta R_n(t) \frac{\partial \zeta[\mathbf{R}]}{\partial R_m} \frac{\partial \zeta[\mathbf{R}]}{\partial R_n} \right\rangle \quad (17)$$

Then, assuming for the sake of simplicity that the diffusion of the atoms in cartesian space is totally uncorrelated, $\langle \Delta R_n(t)\ \Delta R_m(t) \rangle_{(i)} = \delta_{nm}\ 2\ D_n\ t$, yields an estimate of the diffusion constant

$$D(\zeta_b) \simeq \sum_n D_n \left\langle \left(\frac{\partial \zeta[\mathbf{R}]}{\partial R_n} \right)^2 \right\rangle_{(i)} \quad (18)$$

The values of $D(\zeta_b)$ calculated from Eq. 18 assuming a single value for the atomic diffusion constant $D_n = 0.06$ Å^2/ps for all the atoms are reported in Table 5. They are close to the values estimated from the correlation function analysis. This is an indication that the dominant factor determining the magnitude of the diffusion constant is arising from the partial derivative of the reaction coordinate function ($\partial\zeta[\mathbf{R}]/\partial R_n$).

Comparison with experimental results

Experimental information about the dynamics of the dioxolane-linked gating transition were obtained from observations using single-channel recording techniques in GMO/squalene membranes (Stankovic et al., 1989). For the RR isomer, brief closures to zero conductance (flickers) were

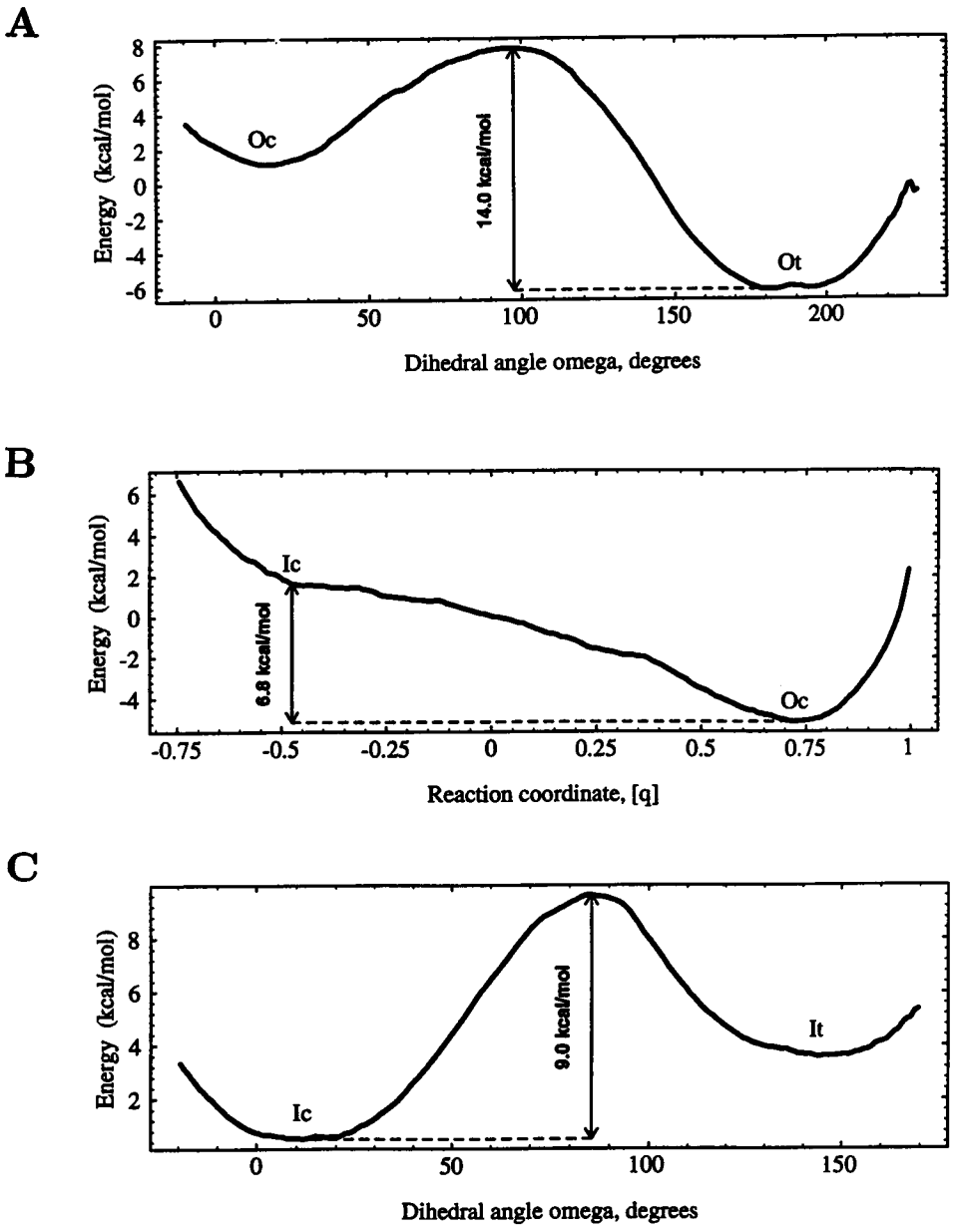

FIGURE 8 PMF for the transition of the RR-linked form from outside to inside the channel. The PMF $W_{out}(\omega)$ (*A*), $W_{cis}(q)$ (*B*), and $W_{in}(\omega)$ (*C*) following the steps Out-*trans* to Out-*cis*, Out-*cis* to In-*cis* and In-*cis* to In-*trans* are shown. The largest activation energies are 14.0 kcal/mol (step Out-*trans* to Out-*cis*) and 6.6 kcal/mol (step Out-*cis* to Out-*trans*).

TABLE 5 Diffusion constants at the barrier top

Transitions	RR-linked form	SS-linked form
$Ot \leftrightarrow Oc$ (degree^2/ps)	860 (840)	1360 (1320)
$Oc \leftrightarrow Ic$ ($[q]^2$/ps)	0.092 (0.024)	0.100 (0.024)
$Ic \leftrightarrow It$ (degree^2/ps)	1280 (1140)	610 (1200)
$It \leftrightarrow Ot$ ($[q]^2$/ps)		0.025 (0.027)

The diffusion constants were calculated using Eq. 14. The numbers in parentheses were calculated using the approximate expression Eq. 18. The partial derivatives $\partial\zeta/\partial R_n$ were calculated by finite difference at the barrier top.

observed during single-channel recordings; the flickers have an average lifetime of ~0.1 ms and occur at a rate of 100/s. No such flickers were observed with the SS isomer. These results are slightly dependent on the membrane preparation. Unpublished results by M. Goeschl, S. Crouzy, and Y. Chapron indicate that the average open and closed time for the RR-linked form are close to 1 ms in POPE and DLPE bilayers.[1] This underlines the important influence the membrane environment may have on the dynamics of the dioxolane ring. Therefore, a perfect quantitative agreement between the experimental observations and the results from the calculations performed in the absence of a lipid membrane is not to be expected.

To relate the results of the calculations with the experimental observations, it is assumed that the channel is able to conduct ions when the dioxolane ring is outside the pore (in the states Out-*trans* or Out-*cis*) and the channel is blocked

[1]Patch clamp experiments were performed on the RR and SS forms of the modified gramicidin using the tip-dip technique of Coronado and Latorre (1983). Dioxolane-linked gramicidin was incorporated into artificial membranes made of a mixture 3:1 of POPE and DLPE (Avanti Polar Lipids, Alabaster, Alabama). Ionic currents measured in symmetrical 640 mM KCl solutions were recorded with a 3-kHz bandwidth.

TABLE 6 Dioxolane transition rates

Transitions		RR-linked form	SS-linked form
Transition Ot ↔ Oc	coordinate ω (degrees)		
Activation energy (kcal/mol)	$\Delta W^{\ddagger}_{Ot\rightarrow Oc}$	14.0	31.3
	$\Delta W^{\ddagger}_{Oc\rightarrow Ot}$	6.6	6.2
Diffusion constant (degree^2/p)	$D(w_b)$	860	1360
Preexponential factor (1/s)	$F_{Ot\rightarrow Oc}$	1.3×10^{12}	6.4×10^{12}
	$F_{Oc\rightarrow Ot}$	1.5×10^{12}	3.5×10^{12}
Rate (1/s)	$k_{Ot\rightarrow Oc}$	70.4	7.0×10^{-11}
	$k_{Oc\rightarrow Ot}$	2.2×10^{7}	1.0×10^{8}
Transition Oc ↔ Ic	coordinate q		
Activation energy (kcal/mol)	$\Delta W^{\ddagger}_{Oc\rightarrow Ic}$		5.6
	$\Delta W^{\ddagger}_{Ic\rightarrow Oc}$		3.8
Diffusion constant (1/ps)	$D(q_b)$		0.10
Pre-exponential factor (1/s)	$F_{Oc\rightarrow Ic}$		4.7×10^{12}
	$F_{Ic\rightarrow Oc}$		5.4×10^{12}
Rate (1/s)	$k_{Oc\rightarrow Ic}$		3.7×10^{8}
	$k_{Ic\rightarrow Oc}$		8.8×10^{9}
Transition It ↔ Ic	coordinate ω (degrees)		
Activation energy (kcal/mol)	$\Delta W^{\ddagger}_{It\rightarrow Ic}$	5.9	3.8
	$\Delta W^{\ddagger}_{Ic\rightarrow It}$	9.0	7.8
Diffusion constant (degree^2/ps)	$D(w_b)$	420	610
Pre-exponential factor (1/s)	$F_{It\rightarrow Ic}$	6.6×10^{11}	1.5×10^{12}
	$F_{Ic\rightarrow It}$	7.8×10^{11}	1.7×10^{12}
Rate (1/s)	$k_{It\rightarrow Ic}$	3.1×10^{7}	2.5×10^{9}
	$k_{Ic\rightarrow It}$	1.9×10^{5}	3.3×10^{6}
Transition Ot ↔ It	coordinate q		
Activation energy (kcal/mol)	$\Delta W^{\ddagger}_{Ot\rightarrow It}$		21.0
	$\Delta W^{\ddagger}_{It\rightarrow Ot}$		13.6
Diffusion constant (1/ps)	$D(q_b)$		0.025
Preexponential factor (1/s)	$F_{Ot\rightarrow It}$		5.4×10^{12}
	$F_{It\rightarrow Ot}$		4.9×10^{12}
Rate (1/s)	$k_{Ot\rightarrow It}$		2.5×10^{-3}
	$k_{it\rightarrow Ot}$		4.1×10^{6}

when the ring is inside the pore (in the states In-*cis* or In-*trans*). In the case of the SS isomer, the limiting step of the most favorable pathway is the transition from the state Out-*trans* to the state Out-*cis*. From the results of Table 6, the estimated blocking rate and average duration of block are 1×10^{-2}/s and 0.06 μs (n.b., it is necessary to multiply the calculated transition rates by a factor of four to account for the multiple pathways). Such short flickers, which could occur once every 100 s, would not be easily detected under normal experimental conditions. This calculation clearly demonstrates that the SS isomer cannot easily flip inside the channel to block the conducting pathway, in qualitative agreement with the experimental results. In the case of the RR isomer, the energetically favorable pathway for the transition from the unblocked to the blocked state was decomposed into three independent steps: Out-*trans* → Out-*cis* → In-*cis* → In-*trans*. The slowest process for blocking the permeation pathway is the transition from the state Out-*trans* to the state Out-*cis*, which corresponds to the isomerization of the peptide bond of Val^1 with the dioxolane outside the channel. The rate-limiting step determining the average lifetime of the blocked state is the transition from the state In-*trans* to the In-*cis* corresponding to the isomerization of the peptide bond of Val^1 with the dioxolane inside the channel. The complex dynamics between the two states In-*cis* and Out-*cis* involves correlated motions of the dioxolane and the hydrogen-bonded chain of the single-file waters and takes place on a shorter time scale. From the results of Table 6, the estimated blocking rate and average duration of block are 280/s and 9 ns (taking account again of the factor of four). Although the blocking rate has approximately the correct magnitude, the lifetime of the blocked channel is much too short and disagrees sharply with the experimental observations.

The underestimated lifetime for the blocked state of the RR form could be due to the inaccuracy of the potential function. For example, the torsional barrier for isomerization of the C—N bond could be misrepresented. Although the C—N torsion is parametrized to yield the correct energy barrier (15 kcal/mol), the empirical potential energy function was not designed to describe such large deviations of the peptide bond from the planar *trans* or *cis* conformation (Brooks et al., 1983). In the force field, the functional form of the C—N torsion corresponds to that of a simple double bond with a two-fold torsion barrier, whereas the true quantum mechanical nature of the energy barrier results from an amide resonance effect that takes place when the π-orbital electrons of the C=O bond are shared with the lone pair of the sp^2-like nitrogen atom (Wiberg and Laidig, 1987). In fact, the nitrogen recovers partly an sp^3-like pyramidal electronic configuration when the N—C=O atoms are not in the same plane (Wiberg and Laidig, 1987). Despite these limitations, the qualitative differences between the SS and RR isomers, which are primarily due to the way they are linked to the native β-helical structure, should be well described by the current force field. Therefore, it is unlikely that inaccuracy of the potential function is the dominant factor, given that the

discrepancy in the transition rate of unblocking corresponds to an increase of approximately 5.5 kcal/mol in the activation energy. An alternative explanation is that the present atomic model does not provide an accurate representation of the true microscopic situation. For example, the calculations were done in the presence of only a small number of single-file waters. Thus the possible influences of bulk water, of phospholipid membrane components, and of the permeating ions were ignored. The influence of the bulk water and the phospholipid membrane on the lifetime of the blocked state would be expected to be small, because of the dioxolane ring location inside the pore (see, e.g., the results obtained for GMO, POPE, and DLPE, above). However, the presence of a permeating K^+ inside the channel could interact strongly with the ring and have a significant influence on the lifetime of the blocked state. The measurements were made in the presence of a relatively high concentration of K^+ ions (640 mM KCl) (Stankovic et al., 1989), and the probability that one K^+ ion is inside the channel at a concentration of 640 mM KCl can be estimated to be ~97% based on an analysis by Heineman and Sigworth (1990). To assess the influence of a K^+ on the dynamics of the dioxolane ring, additional PMFs were calculated in the presence of one K^+ ion inside the gramicidin channel.

TABLE 7 Dioxolane transition rates of the RR form in the presence of K^+

Transitions		RR-linked form
Transition It ↔ Ic	coordinate ω (degrees)	
Activation energy (kcal/mol)	$\Delta W^{\ddagger}_{Ic\to It}$	12.2
	$\Delta W^{\ddagger}_{Ic\to It}$	6.4
Diffusion constant (degrees^2/ps)	$D(w_b)$	1280
Pre-exponential factor (1/s)	$F_{It\to Ic}$	5.3×10^{12}
	$F_{Ic\to It}$	5.5×10^{12}
Rate (1/s)	$k_{It\to Ic}$	5.9×10^{3}
	$k_{Ic\to It}$	1.1×10^{8}

Calculations, as reported in Fig. 9 and in Table 7, were also done for the RR form with a K^+ ion replacing a single-file water in the center of the channel. The PMF for the path from state In-*trans* to state In-*cis* is shown in Fig. 9 together with the PMF calculated with no ion; the results are summarized in Table 7. The contribution of the K^+ ion to the PMF corresponding to the transition from In-*cis* to Out-*cis* has also been computed, and the PMF is shown in Fig. 9 together with the PMF obtained with no ion. The isomerization of the peptide bond with the dioxolane ring inside the channel appear to remain the rate-limiting event determining the lifetime of the blocked state. Although the relative stability of the In-*cis*

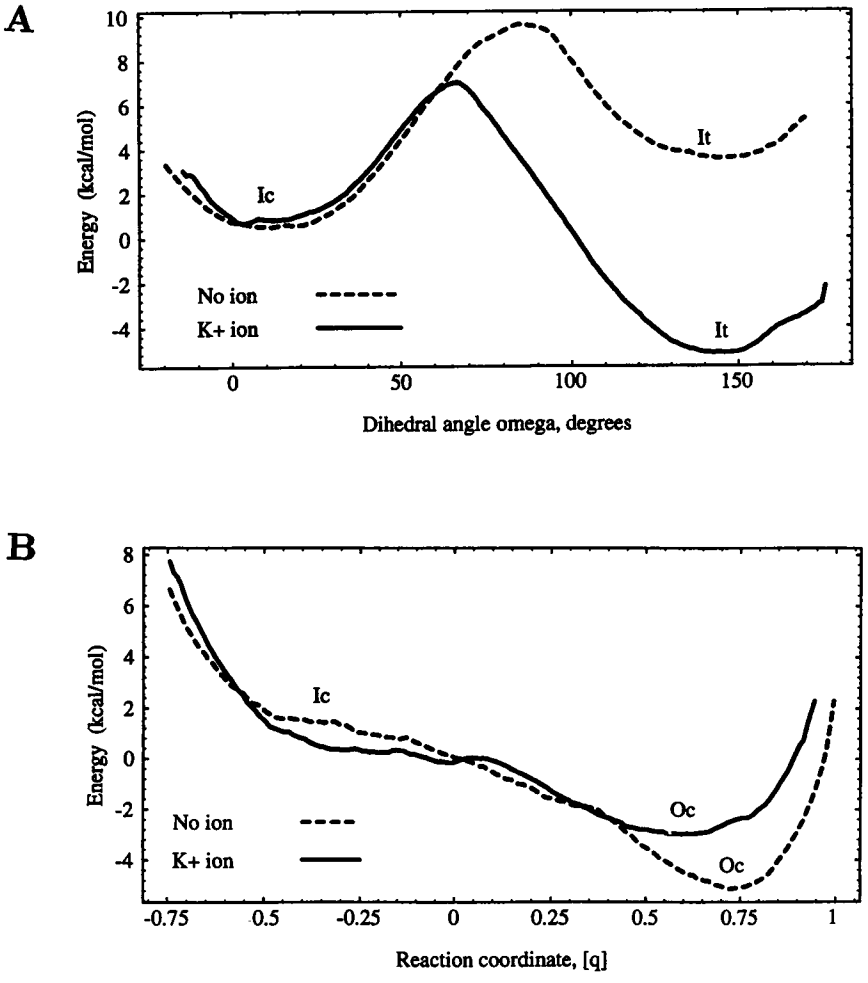

FIGURE 9 Influence of a K^+ ion inside the channel on the PMF of the RR-linked form. The PMF $W_{in}(\omega)$ (*A*) and $W_{cis}(q)$ (*B*) calculated with and without ion inside the channel are shown for the transition In-*cis* to In-*trans* and In-*cis* to Out-*cis*. The presence of a K^+ ion inside the channel near the ring, stabilizes the ω dihedral angle in the *trans* configuration by 6 kcal/mol.

and Out-*cis* states appears to be slightly affected by the presence of the cation (the energy well corresponding to the state Out-*cis* is now 3.4 kcal/mol less deep than without K^+), the state In-*cis* corresponds to a very shallow free-energy well as in the calculation with no cation. It is observed that the presence of a K^+ ion near the center of the channel stabilizes significantly the dioxolane ring in the In-*trans* conformation. The activation energy barrier changes from 5.9 kcal/mol in the water-filled channel to 12.2 kcal/mol when a K^+ ion is present. Based on the results shown in Table 7, the estimated lifetime of the blocked state in the presence of a permeating K^+ inside the channel is 0.04 ms, much closer to the experimental value. Based on the calculated PMF, the RR isomer spends nearly 97% of its time outside the channel and only 3% inside. This result is in good accord with the block fraction observed experimentally (1% for the RR-linked channel) (Stankovic et al., 1989). The present estimate of the influence of a K^+ ion on the lifetime of the blocked state is restricted to a single location near the center of the channel. Although it is possible to consider different positions for the K^+ in the channel, extension of the present calculations to investigate fully the permeation process through the linked channels, such as the calculations of the free-energy profile (Roux and Karplus, 1993), would be very intensive computationally.

CONCLUSION

The present study represents one of the first applications of molecular dynamics methods to study the gating of an ion channel. Based on an atomic model of the dioxolane ring-linked gramicidin channel, a reaction scheme was proposed and the corresponding transition rates were calculated using specialized computational techniques for biased sampling. An important finding of this investigation is that the gating transition of the RR-linked dioxolane ring inside the channel is facilitated considerably if the peptide bond dihedral angle of Val^1 first undergoes a *trans*-to-*cis* isomerization. Along the most favorable pathway, the activation energy of the SS form is much larger than that of the RR form, and the calculated gating transition rate constants appear to be in good accord with the experimentally measured lifetimes of the open and of the blocked states of the channel. However, several aspects of the system were neglected to allow extensive configurational sampling required by the computational approach. In particular, the membrane environment of a phospholipid bilayer was ignored, and only a small number of single-file water molecules were included in the calculations. Furthermore, the force field used was not designed to describe large deviations of the peptide bond from the *trans* or *cis* planar conformation. Finally, the effect of a permeant ion inside the channel on the gating was considering the presence of a K^+ ion at only a single location, near the center of the channel. Nevertheless, several conclusions can be drawn from the present study despite these limitations.

First, the present work illustrates the difficulty of finding an appropriate reaction coordinate to describe a conformational change in a complex macromolecular system. Because there is usually little information available from experiments about the transition state corresponding to an allosteric conformational change in a protein, it is necessary to deduce the reaction coordinate function $\zeta[\mathbf{R}]$ from a theoretical approach. There are no simple rules to choose a reaction coordinate for the purpose of describing dynamical properties in a complex multidimensional system (Hynes, 1985), although it is desirable to choose a conceptually simple function $\zeta[\mathbf{R}]$ to be able to perform the biased configurational sampling with molecular dynamics simulations. Well motivated choices can be deceptively inadequate. For example, the initial choice of the coordinate $q[\mathbf{R}]$, varying from -1 (ring inside) to $+1$ (ring outside) seemed to describe well the transition of the dioxolane ring from outside to inside the channel. However, it became clear during preliminary calculations that a significant structural rearrangement involving the *trans*-to-*cis* isomerization of the peptide bond of Val^1 was also participating in the transition. During these preliminary explorations, multidimensional adiabatic surfaces can give useful information for making progress in elucidating the mechanism of a conformational transition and choosing the reaction coordinate function. In the present work, such surfaces were used to identify the four stable states of the dioxolane-linked channels and to find the energetically favorable transition pathways allowing the passage of the ring from outside to inside the channel. Nevertheless, an adiabatic surface provides only an approximate picture to the real dynamics of the system at room temperature, because it is based on the assumption that all degrees of freedom other than q and ω are at their energy minimum. For example, the state In-*cis* of the RR-linked form, which corresponds to a stable configuration on the adiabatic energy surface, was not stable in the presence of single-file waters. The biased sampling simulations can reveal further difficulties, e.g., the breaking of the hydrogen-bonded single file of water molecules to allow the transition of the ring inside the channel suggests that a further refinement of the reaction coordinate function could also include the position of these waters as well. In future applications of the present approach to calculating transition rate constants between different conformations of complex biological macromolecules, it may be necessary to follow a similar route and proceed by trial and error. The recently developed computational techniques to find reaction paths of least energy may be helpful (Choi and Elber, 1991; Fischer and Karplus, 1992).

Secondly, the present work illustrates the fundamental importance of representing the true microscopic situation correctly for a valid comparison of calculations based on an atomic model with experimental observations. In the present study, the presence of a K^+ ion close to the ring has been necessary to reproduce the experimentally observed lifetime of the blocked channel. This result is not surprising, given that the channel is believed to be almost always occupied by at least one ion. It also raises the experimental question of how the transition rate for the ring flip depends on the ion concentration. More generally, it may be expected that the

presence of permeating ions can influence gating transitions within more complex biological channels. The ionic current, which is used to probe the gating dynamics of macromolecular channel structures, is also responsible for the presence of permeating ions near the very atomic groups that are involved in the gating transition. The interactions of permeant ions with the channel structure and its influence on the gating kinetics was first reported by Marchais and Marty (1979) for channels activated by acetylcholine in *Aplysia* neurones. Complex gating phenomena have been observed, channels can close more slowly in the presence of external K^+ and Rb^+ (Swenson and Armstrong, 1981), or, e.g., K are stabilized in the closed state by the presence of Ba^{2+} ions (Armstrong et al., 1982) or stabilized in the open state (by 1.2 kcal/mol) when Ba^{2+} is used as permeant ion relative to K^+ (Miller et al., 1987). The influence of permeant ion-channel interactions on the gating kinetics should be considered in trying to deduce the elementary processes responsible for the function of ligand-gated and voltage-gated channels on the basis of single-channel recordings and gating current measurements together with site-directed mutagenesis (Armstrong, 1992; Bezanilla and Stühme, 1989; Bezanilla et al., 1991; Sigworth, 1994).

The present calculations suggest new experimental investigations of dioxolane-linked gramicidin channels. In particular, according to the proposed reaction scheme, patch clamp measurements with a better time resolution could reveal an eventual second component in the open lifetime in the μs time range. In addition, it would be interesting to investigate the structure and dynamics of the dioxolane ring in the linked channels using spectroscopic methods such as two-dimensional NMR in SDS micelles (Arseniev et al., 1985) or solid-state NMR in oriented bilayers (Nicholson and Cross, 1989). For example, it may be possible to detect the *trans-cis* isomerization of the peptide bond of Val^1 in dioxolane-linked channel from measurements of vicinal J-coupling constants or from nuclear Overhauser effects.

We are grateful to Jean Luc Douville for his help in the production of surface and contour plots. This investigation was begun when S. Crouzy and T. B. Woolf were working in the laboratory of F. J. Sigworth. We are grateful for his support.

REFERENCES

Andersen, O. S. 1984. Gramicidin channels. *Ann. Rev. Physiol.* 46: 531–548.

Andersen, O. S., and R. E. Koeppe II. 1992. Molecular determinants of channel function. *Physiol. Rev.* 72:S89–158.

Armstrong, C. M. 1981. Sodium channels and gating currents. *Physiol. Rev.* 61:644–683.

Armstrong, C. M. 1992. Voltage-dependent ion channels, and their gating. *Physiol. Rev.* 72, S5–13.

Armstrong, C. M., R. P. Swenson, and S. R. Taylor. 1982. Block of squid axon K-channels by internally, and externally applied Barium ions. *J. Gen. Physiol.* 80:663–682.

Arseniev, A. S., V. F. Bystrov, T. V. Ivanov, and Y. A. Ovchinnikov. 1985. ^{1}H-NMR study of gramicidin-A transmembrane ion channel. Head-to-head right-handed, single stranded helices. *FEBS Lett.* 186:168–174.

Auerbach, A. 1993. A statistical analysis of acetylcholine receptor activation in *Xenopus* myocytes: stepwise vs. concerted models of gating. *J. Physiol.* 461:339–378.

Berne, B. J., M. Borkovec, and J. E. Straub. 1988. Classical and modern methods in reaction rate theory. *J. Phys. Chem.* 92:3711–3725.

Bezanilla, F., and W. Stühmer. 1989. Quantal charge redistribution accompanying the structural transition of sodium channels. *Eur. Biophys. J.* 17:53–59.

Bezanilla, F., E. Perozo, D. M. Papazian, and E. Stefani. 1991. Molecular basis of gatin charge immobilization in *Shaker* potassium channels. *Science.* 254:679–683.

Briggs, J. M., T. Matsui, and W. L. Jorgensen. 1990. Monte Carlo simulations of liquid alkyl ethers with the OPLS potential functions. *J. Comput. Chem.* 11:958–971.

Brooks, B. R., R. E. Bruccoleri, B. D. Olafson, D. J. States, S. Swaminathan, and M. Karplus. 1983. CHARMM: A program for macromolecular energy minimization, and dynamics calculations. *J. Comput. Chem.* 4: 187–217.

Brooks, C. L. III, M. Karplus, and B. M. Pettitt. 1988. Proteins. A theoretical perspective of dynamics, structure, and thermodynamics. *In* Advances in Chemical Physics, Vol. 71. I. Prigogine and S. A. Rice, editors. John Wiley Sons, New York.

D. Chandler. 1987. Introduction to Modern Statistical Mechanics. Oxford University Press, Oxford, U.K.

Chiu S. W., E. Jakobsson, S. Subramaniam, and J. A. McCammon. 1991. Time-correlation analysis of simulated water motion in flexible, and rigid gramicidin channels. *Biophys. J.* 60:273–285.

Chiu, S. W., S. Subramaniam, E. Jakobsson, and J. A. McCammon. 1989. Water, and polypeptide conformations in the gramicidin channel. *Biophys. J.* 56:253–261.

Choi, C., and R. Elber. 1991. Reaction path study of helix formation in tetrapeptides: effects of side chains. *J. Chem. Phys.* 94:751–760.

Coronado, R., and R. Latorre. 1983. Phospholipid bilayers made from monolayers on patch clamp pipette. *Biophys. J.* 43:231–236.

Cremer, D., and J. A. Pople. 1975. A general definition of ring puckering coordinates. *J. Am. Chem. Soc.* 97:1354–1358.

Crouzy, S., T. B. Woolf, and B. Roux. 1992. Molecular dynamics exploration of gating in dioxolane ring linked gramicidin. *Biophys. J.* 61:A525.

Durrel, S. R., and H. R. Guy. 1992. Atomic scale structure, and functional models of voltage-gated potassium channels. *Biophys. J.* 62:238–250.

Finkelstein, A., and O. S. Andersen. 1981. The gramicidin A channel: a review of its permeability characteristics with special reference to the single-file aspect of transport. *J. Memb. Biol.* 59:155–171.

Fischer, S., and M. Karplus. 1992. Conjugate peak refinement: an algorithm for finding reaction paths, and accurate transition states in systems with many degrees of freedom. *Chem. Phys. Lett.* 194:252–261.

Glasstone, S., K. J. Laidler, and H. Eyring. *Theory of Rate Processes.* McGraw-Hill, New York, 1941.

Guy, H. R., and F. Conti. 1990. Pursuing the structure, and function of voltage-gated channels. *Trends Neurosci.* 13:201–206.

Haydock, C., J. C. Sharp, and F. G. Prendergast. 1990. Tryptophane-47 rotational isomerization in variant-3 scorpio neurotoxin. A combination thermodynamic perturbation, and umbrella sampling study. *Biophys. J.* 57:1269–1279.

Heinemann, S. H., and F. J. Sigworth. 1990. Open channel Noise V. A fluctuating barrier to ion entry in gramicidin A channels. *Biophys. J.* 57:499–514.

Hille, B. 1984. Ionic Channels of Excitable Membranes. Sinauer, Sunderland MA.

Hynes, J. T. 1985. The theory of reactions in solutions. *In* Theory of Chemical Reaction Dynamics. M. Baer, editor. CRC Press, Boca Raton, FL. 171–235.

Jorgensen, W. L., J. D. Madura, J. Chandrasekhar, R. W. Impey, and M. L. Klein. 1983. Comparison of simple potential functions for simulating liquid water. *J. Chem. Phys.* 79:926–935.

Kramers, H. A. 1940. Brownian motion in a field of force, and the diffusion model of chemical reactions. *Physica.* 7:284–304.

Läuger, P. 1973. Ion transport through pores: a rate theory analysis. *Biochim. Biophys. Acta.* 311:423–441.

Marchais, D., and A. Marty. 1979. Interaction of permeant ions with channels activated by acetylcholine in *Aplysia* Neurones. *J. Physiol.* 297:9–45.

McCammon, J. A., and M. Karplus. 1979. Dynamics of activated processes

in globular proteins. *Proc. Natl. Acad. Sci. USA* 76:3585–3589.

Miller, C., R. Latorre, and I. Reisin. 1987. Coupling of voltage-dependent gating, and Ba^{++} block in the high-conductance Ca^{++}-activated K^+ channel. *J. Gen. Physiol.* 90:427–449.

Neher, E., and B. Sackmann. Single-channel currents recorded from membrane of denervated frog muscle fibers. *Nature.* 260:779–802 1976.

Nicholson, L. K., and T. A. Cross. 1989. The gramicidin cation channel: an experimental determination of the right-handed helix sense, and verification of β-type hydrogen bonding. *Biochemistry.* 28:9379–9385.

Northrup, S. H., M. R. Pear, C. Y. Lee, J. A. McCammon, and M. Karplus. 1982. Dynamical theory of activated processes in globular proteins. *Proc. Natl. Acad. Sci. USA.* 79:4035–4039.

Patey, G. N., and J. P. Valeau. 1975. A Monte Carlo method for obtaining the interionic potential of mean force in ionic solution. *J. Chem. Phys.* 63:2334–2339.

Reiher, W. E. 1985. Theoretical studies of hydrogen bonding. Ph.D. thesis. Harvard University, Cambridge, Massachusetts.

Roux, B., and M. Karplus. 1991a. Ion transport in a model gramicidin channel: structure and thermodynamics. *Biophys. J.* 59:961–981.

Roux, B., and M. Karplus. 1991b. Ion transport in a gramicidin-like channel: dynamics and mobility. *J. Phys. Chem.* 95:4856–4868.

Roux, B., and M. Karplus. 1993. Ion Transport in the gramicidin channel: free energy of the solvated right-handed dimer in a model membrane. *J. Am. Chem. Soc.* 115:3250–3262.

Roux, B., and M. Karplus. 1994a. Molecular dynamics simulations of the gramicidin channel. *Annu. Rev. Biomol. Struc. Dyn.* 23:731–761.

Roux, B., and M. Karplus. 1994b. Empirical energy function for cations-peptides interactions. *J. Comput. Chem.* In press.

Ryckaert, J. P., G. Ciccotti, and H. J. C. Berendsen. 1977. Numerical integration of the cartesian equation of motions of a system with constraints: molecular dynamics of *n*-alkanes. *J. Comput. Chem.* 23:327–341.

Seoh, S., and D. Busath. 1993. Formamidinium-induced dimer stabilization, and flicker block behavior in homo- and heterodimer channels formed by gramicidin A, and *N*-acetyl gramicidin A. *Biophys. J.* 65:1817–1827.

Sigworth, F. J. 1994. Voltage gating of ion channels. *Q. Rev. Biophys.* 27:1–40.

Stankovic, C. J., S. H. Heinemann, J. M. Delfino, F. J. Sigworth, and S. L. Schreiber. 1989. Transmembrane channels based on tartaric acid-gramicidin a hybrid. *Science.* 244:813–817.

Stefani, E., L. Toro, E. Perozo, and F. Bezanilla. 1994. Gating of *Shaker* K^+ channels: I. Ionic and gating current. *Biophys. J.* 66:996–1010.

Straub, J., and B. J. Berne. 1988. Molecular dynamics study of an isomerizing diatomic in a Lennard-Jones fluid. *J. Chem. Phys.* 89:4833–4847.

Swenson, R. P., and C. M. Armstrong. 1981. K^+ channels close more slowly in the presence of external K^+, and Rb^+. *Nature Lond.* 291:427–429.

Szabo, G., and D. W. Urry. 1978. *N*-acetyl gramicidin: single-channel properties and implications for channel structure. *Science.* 203:55–57.

Urry, D. W. 1971. The gramicidin A transmembrane channel: a proposed π_{LD} helix. *Proc. Natl. Acad. Sci. USA.* 68:672–676.

Wiberg, K. B., and K. E. Laidig. 1987. Barriers to rotation adjacent to double bonds. 3. The C-O barrier in formic acid, methyl formate, acetic acid, and methyl acetate. The origin of ester, and amide "resonance". *J. Am. Chem. Soc.* 109:5935–5943.

Wooley, G. A., and B. A. Wallace. 1992. Model ion channels: gramicidin and alamethicin. *J. Membr. Biol.* 129:109–136.

Woolf, T. B., and B. Roux. 1994. The conformational flexibility of *o*-phosphorylcholine, and *o*-phosphorylethanolamine: a molecular dynamics study of solvation effects. *J. Am. Chem. Soc.* 116: 5916–5926.